

Appendix

Inner-ear circulation in humans is disrupted by extracranial venous outflow strictures: implications for Ménière's disease

Eleuterio F. Toro, Francesco Borgioli, Qinghui Zhang, Christian Contarino, Lucas Omar
Müller, Aldo Bruno

Appendix

Here we have extended the Müller-Toro mathematical model.^{1,2} This is a global multiscale model that places particularly emphasis on the venous system; it includes a 1D description of all major blood vessels and 0D compartmental models for the microcirculation, the heart, the pulmonary circulation and the CSF compartment.

1D Equations

For major vessels the 1D averaged equations read:

$$\partial_t A + \partial_x q = 0 \quad (1)$$

$$\partial_t q + \partial_x \left(\frac{q^2}{A} \right) + \frac{A}{\rho} \partial_x p = -f \quad (2)$$

where x is the axial coordinate, t is time, $A = A(x, t)$ is the cross-sectional area, $q = q(x, t)$ is the cross-sectional area averaged flow rate, $p = p(x, t)$ is the averaged internal pressure, ρ is the, constant, blood density and $f(x, t)$ is friction force per unit length, with $f = 8\pi\mu u/\rho$, where μ is blood kinematic viscosity and u is velocity. Note that $q(x, t) = A(x, t)u(x, t)$. To close the system of equations we introduce the tube law:

$$p(x, t) = p_e(x, t) + K(x)\varphi((A(x, t), A_0(x)) + P_0. \quad (3)$$

Here $p_e(x, t)$ is the external pressure; $A_0(x)$ is the equilibrium cross-sectional area; P_0 is the reference pressure when $A = A_0$ and $u(x, t) = 0$; $K(x)$ is a positive function depending on the geometrical and mechanical properties of the blood vessels. Both $K(x)$ and the function φ assume different expressions to differentiate between arteries and veins. For further details

on the tube laws for arteries and veins see ^{1,2} and Appendix Table 1.³⁻⁶ The numerical solution of the system of equations is computed with a high-order ADER⁷ numerical scheme. For background on ADER see Chaps. 19 and 20 of⁸. The method consists of a non-linear spatial reconstruction step followed by the solution of the Generalized Riemann Problem⁹ at each cell interface to compute the numerical flux. Here we use Dumbser-Enaux-Toro solver¹⁰ to solve this problem and the Dumbser-Osher-Toro Riemann solver¹¹ to solve the classical Riemann problem, also needed to solve the Generalized Riemann Problem.

0D Equations

In this paper we have added 0D compartments to account for the inner ear microcirculation, associated to the 1D vessels introduced in the model. These models are obtained by firstly linearizing the 1D system about the reference state ($A = A_0, p = 0, q = 0$) and then integrating over the length of the vessel of interest leading to the ODEs:

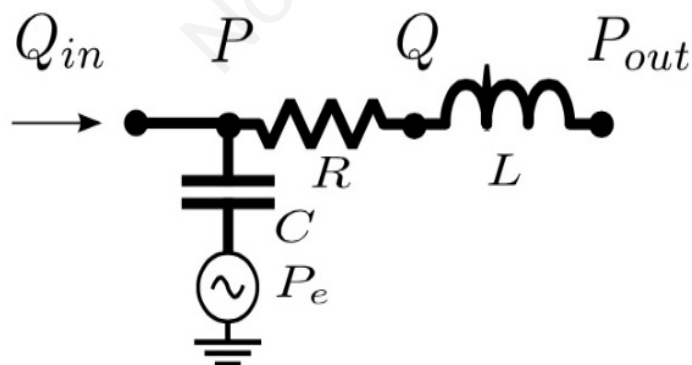
$$C \frac{dP}{dt} + Q - Q_{in} = 0, \quad (4)$$

$$L \frac{dQ}{dt} + RQ + P_{out} - P = 0, \quad (5)$$

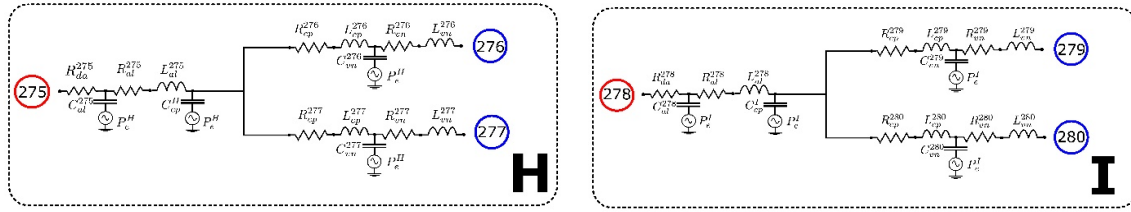
where $P(t), Q(t)$ are the state variables of the lumped compartment, *i.e.* pressure and flow rate, and P_{out}, Q_{in} are variables related to adjacent compartments or obtained by the imposed boundary conditions. Moreover, the coefficient R, L, C are specific to the compartment of interest, corresponding to the viscous resistance to flow, blood inertia and wall compliance, respectively. These coefficients are defined as follows:

$$R = l \frac{8 \mu}{R_0^4 \pi}, L = l \frac{\rho}{A_0}, C = l \frac{A_0}{\rho c_0^2}, \quad (6)$$

where l is the vessel length, μ is the blood viscosity and ρ the blood density. Since in our compartmental models are used for the microcirculation, we also take into account the number of vessels (that is the number of arterioles per artery, the number of capillaries per arteriole and the number of venules per capillary) in order to correctly compute the coefficient of every compartment, since coefficients have been calculated considering a system of vessels in parallel.¹² The configuration of every compartment is as represented in Appendix Figure 1, and describes the arteriolar, the capillar or the venular district. For details on the approach see ². In the present work, two new 0D models have been added to investigate the inner ear microvasculature; the new compartments connect the anterior inferior cerebellar arteries to the LABVs and to the VCAQs. Their configuration is represented in Appendix Figure 2: two different capillary networks have been defined in order to distinguish the cochlear microcirculation from the vestibular one. Parameters for all the compartments in the model are given in Appendix Table 2.^{13,14}



Appendix Figure 1. Single lumped compartment: the combination of several compartments constitutes a 0D model for the microcirculation.



Appendix Figure 2. Right (H) and left (I) lumped compartments for the inner ear circulation. This configuration has been used in order to distinguish the cochlear capillaries (vessels 276, 279) from the vestibular capillaries (vessels 277, 280). For details on vessel numbering see ^{1,2}.

Appendix Table 1. Geometrical properties of the vessels modified or introduced into the original Müller-Toro model^{1,2} to carry the present study.

No.	Vessel name	L [cm]	r_0 [cm]	r_1 [cm]	c_0 [cm]	Loc	Ref
56	Basilar art. I	0.960	0.1620	0.1620	9.33	1	³
274	Basilar art. II	1.930	0.1620	0.1620	9.33	1	³
275	R. ant. inf. cerebellar art.	1.400	0.0400	0.0650	23.77	1	⁴
278	L. ant. inf. cerebellar art.	1.400	0.0400	0.0650	23.77	1	⁴
276	R. vein of the cochlear aq. I	0.645	0.0100	0.0100	3.00	9	⁵
277	R. labyrinthine vein I	0.433	0.0375	0.0375	2.99	9	⁶
279	L. vein of the cochlear aq. I	0.645	0.0100	0.0100	3.00	9	⁵
280	L. labyrinthine vein I	0.433	0.0375	0.0375	2.99	9	⁶
281	R. vein of the cochlear aq. II	0.645	0.0100	0.0100	3.00	9	⁵
282	R. labyrinthine vein II	0.433	0.0375	0.0375	2.99	9	⁶
283	L. vein of the cochlear aq. II	0.645	0.0100	0.0100	3.00	9	⁵
284	L. labyrinthine vein II	0.433	0.0375	0.0375	2.99	9	⁶

L: length; r_0 reference inlet radius; r_1 : reference outlet radius; c_0 : wave speed in the reference configuration; Loc: location in the body; Ref: bibliographic source.

Table 2. Parameters for the 0D compartments included in the model. The first column shows the indexes of the (parent) artery and the (daughter) veins. The second column shows the distal arteries R_{da} [mmHg s mL⁻¹] while the remaining columns give resistance R [mmHg s mL⁻¹], inductance L [mmHg s² mL⁻¹] and capacitance C [mmHg⁻¹ mL] for arterioles, and venules respectively. Capacitances were computed as $C_2 = 0.1C_1$, $C_3 = 3C_1$, as in ¹³. Parameters for the new compartments H and I were obtained from data in ^{12,14}.

Parent/daughter vessel	R_{da}	R_{al}	L_{al}	C_{al}	R_{cp}	L_{cp}	C_{cp}	R_{vn}	L_{vn}	C_{vn}
Lumped Model H										
275	4.700*10	7.153	4.735*10 ⁻⁴	3.738*10 ⁻⁵	-	-	-	-	-	-
Common param.	-	-	-	-	-	-	3.738*10 ⁻⁶	-	-	-
276	-	-	-	-	3.260	1.365*10 ⁻⁵	-	4.828	1.420*10 ⁻⁴	1.218*10 ⁻⁴
277	-	-	-	-	3.260	1.365*10 ⁻⁵	-	4.828	1.420*10 ⁻⁴	1.218*10 ⁻⁴
Lumped Model I										
278	4.700*10	7.153	4.735*10 ⁻⁴	3.738*10 ⁻⁵	-	-	-	-	-	-
Common param.	-	-	-	-	-	-	3.738*10 ⁻⁶	-	-	-
279	-	-	-	-	3.260	1.365*10 ⁻⁵	-	4.828	1.420*10 ⁻⁴	1.218*10 ⁻⁴
280	-	-	-	-	3.260	1.365*10 ⁻⁵	-	4.828	1.420*10 ⁻⁴	1.218*10 ⁻⁴

References

1. Müller LO, Toro EF. A global multiscale mathematical model for the human circulation with emphasis on the venous system. *J Numer Method Biomed Eng* 2014;30:681-725.
2. Müller LO, Toro EF. An enhanced closed-loop model for the study of cerebral venous blood flow. *J Biomech* 2014;47:3361-72.
3. Liang FY, Fukasaku K, Liu H, et al. A computational model study of the influence of the anatomy of the circle of willis on cerebral hyperperfusion following carotid artery surgery. *Biomed Eng Online* 2011;10.
4. Habibi Z, Meybodi AT, Maleki F, et al. Superior and anterior inferior cerebellar arteries and their relationship with cerebello-pontine angle cranial nerves revisited in the light of cranial cephalometric indexes: a cadaveric study. *Turkish Neurosurgery* 2011;21:504-15.
5. Pellet W, Cannoni M, Pech A. *Otoneurology*. Berlin: Springer-Verlag; 1990.
6. Chen H, Yu Y, Zhong S, et al. Three-dimensional reconstruction of internal auditory meatus and anatomical study of the inner structures. *Zhonghua Er Bi Yan Hou Ke Za Zhi* 2000;35:204-6.
7. Toro EF, Millington RC, Nejad LAM. Towards very high-order Godunov schemes. In *Godunov methods: theory and applications*. New York: Kluwer Academic/Plenum Publishers; 2001. pp 905-37.
8. Toro EF. *Riemann solvers and numerical methods for fluid dynamics. A practical introduction*, 3rd edition. Berlin-Heidelberg: Springer-Verlag; 2009.
9. Toro EF, Titarev VA. Solution of the generalized Riemann problem for advection-reaction equations. *Proc R Soc A* 2002;358:271-81.
10. Dumbser M, Eaux C, Toro EF. Finite volume schemes of very high order of accuracy for stiff hyperbolic balance laws. *J Comput Phys* 2008;227:3971-4001.

11. Dumbser M, Toro EF. On universal osher-type schemes for general nonlinear hyperbolic conservation laws. *Comm Comput Phys* 2011;10:635-71.
12. Kurbel S, Gros M, Maric S. Complexity of human circulation design: tips for students. *Adv Physiol Educ* 2009;33:130-1.
13. Liang FY, Takagi S, Himeno R, et al. Biomechanical characterization of ventricular-arterial coupling during aging: a multi-scale model study. *J Biomech* 2009;42:692-704.
14. Silverthorn DU. *Human physiology: an integrated approach*, 5th edition. San Francisco: Pearson/Benjamin Cummings; 2010.

Non-commercial use only